metals

MDPI

Article

Temperature Dependency of Modified Mohr–Coulomb Criterion Parameters for Advanced High Strength Dual-Phase Steel DP780

Yukuan Li, Di Li *, Hui Song, Yiqun Wang and Dongze Wu

School of Traffic and Vehicle Engineering, Shandong University of Technology, Zibo 255000, China; 18763941690@163.com (Y.L.); 17853314102@163.com (H.S.); w826433163@sina.cn (Y.W.); 18249877310@163.com (D.W.)

* Correspondence: hahali@sdut.edu.cn

Abstract: The Modified Mohr–Coulomb criterion has been demonstrated to exhibit high accuracy in the prediction of fracture in high-strength steels. Taking DP780 as the research object, the undetermined parameters of the Modified Mohr–Coulomb criterion at different temperatures were calibrated by tensile and shear tests combined with simulation. The relationships between the parameters and temperature were investigated. Finally, the relationship between criterion parameters and temperature was verified using the stretch-bending tests of U-shape parts. The fracture of automotive parts can be accurately predicted by simulation during warm stamping, thereby guiding actual production.

Keywords: advanced high strength dual-phase steel; modified Mohr–Coulomb criterion; DP780; stress triaxiality; temperature dependency

check for updates

Citation: Li, Y.; Li, D.; Song, H.; Wang, Y.; Wu, D. Temperature Dependency of Modified Mohr–Coulomb Criterion Parameters for Advanced High Strength Dual-Phase Steel DP780. *Metals* **2024**, *14*, 721. https://doi.org/10.3390/met14060721

Academic Editor: Antonio Mateo

Received: 9 May 2024
Revised: 9 June 2024
Accepted: 14 June 2024
Published: 17 June 2024

Copyright: © 2024 by the authors. Licensee MDPI, Basel, Switzerland. This article is an open access article distributed under the terms and conditions of the Creative Commons Attribution (CC BY) license (https://creativecommons.org/licenses/by/4.0/).

1. Introduction

Advanced high-strength dual-phase steels exhibit the advantages of high energy absorption capacity, easy press molding, good plastic ductility, etc. In recent decades, the automotive industry has witnessed a surge in the use of advanced high-strength dual-phase steels, driven by the twin demands of weight reduction and passive safety [1]. These steels have been employed extensively in automotive structural components, reinforcing parts, and other components [2]. In recent years, the relative difficulty of the cold press forming of high-strength steel has prompted numerous scholars to apply the warm forming technology to the field of high-strength steel. The implementation of high-strength steel warm forming technology not only enables the lightweight construction of automobiles but also significantly enhances the passive safety performance of the car, which has become an important forming process [3].

Ductile fracture is a common failure mode when forming complex components of high-strength steel plates, particularly in the vicinity of the material near the punch and die fillet, which is prone to shear fracture without clear evidence of material necking [4]. This type of fracture is challenging to accurately predict using conventional forming limit diagrams based on material necking failure. A growing body of research is focusing on the prediction of fracture behavior in high-strength steels using the ductile fracture criterion [5]. The ductile fracture model "Modified Mohr-Coulomb criterion" (MMC) is more widely used to predict the shear fracture damage of dual-phase steels due to its favorable computational stability, the necessity of identifying a smaller number of parameters, and the simplicity of identification based on experimental data [6]. Bai and Wierzbicki introduced the generalized hardening criterion [7] of their study, which modifies the Mohr–Coulomb criterion in the geotechnical field. They also proposed the Modified Mohr–Coulomb criterion (MMC) [8], which better simulates the brittle fracture and ductile failure of metallic materials [9]. Ji, C [10] developed an improved MMC fracture model to characterize the anisotropic and strain rate-dependent fracture characteristics of aluminum alloys. The reliability of the criterion was verified through a combination of experiments

and simulations. Granum H [11] proposed a calibration method for the MMC fracture model based on localization analysis and applied it to AA6016 aluminum alloy, reducing the number of mechanical tests required to calibrate the MMC fracture model. The MMC criterion proposed by Bai and Wierzbicki was based on aluminum alloy materials and was subsequently extended to DP steels. Meng L [12] analyzed the fracture failure behavior of dual-phase steel plate material during the stretch-bending forming process by using the MMC criterion. Pack K [13] predicted the fracture process of TRIP780 high-strength steel using the MMC fracture model. In a study by Dunand [14], the predictions were compared to the TRIP 780 steel fracture experiments. The MMC model was found to correctly predict the fracture. Huang G [15] predicted the fracture mechanical behavior of hot-formed steel by employing the MMC fracture model. Lou [16] employed the MMC criterion to investigate the fracture behavior of high-strength steel under diverse stress triaxiality conditions. This approach enables a more precise characterization of the ductile behavior of metals across a range of stress states, encompassing shear, plane strain tension, and beyond. A review of the literature reveals that the MMC criterion can predict the fracture behavior of high-strength steels with greater accuracy than other criteria. However, the majority of studies have been conducted at room temperature, and there is a paucity of research investigating the relationship between the MMC criterion and temperature in order to predict rupture under warm forming conditions. Consequently, this paper concentrates on the temperature dependence of the MMC criterion under warm forming conditions (298 K–873 K) for the DP780 sheet, with the MMC criterion employed to predict rupture under high-temperature conditions.

In this paper, uniaxial tensile and shear tests were conducted on DP780 at different temperatures. The plastic behavior and ductile fracture properties of the steel plates were comprehensively characterized using Hill's orthogonal anisotropic elastic–plastic model and the MMC fracture criterion. The numerical simulation program was prepared using the Abaqus Explicit user material subroutine and compared to the test results. The objective of this study was to determine the fracture criterion parameters of DP780 at temperatures ranging from 298 K to 873 K and to investigate the relationship between these parameters and temperature.

2. MMC Model

Wierzbicki [7] proposed a strain-modified Mohr-Coulomb (MMC) fracture prediction model, which is an extension of the maximum shear stress criterion that is widely used for shear-type failure, and it can effectively predict shear-type fracture in the steel plate forming process. Moreover, the MMC criterion has fewer parameters to be determined and is more convenient to apply. The macroscopic mechanical MMC fracture criterion can be expressed as follows:

$$D = \int_0^{\bar{\varepsilon}_f} \frac{d\bar{\varepsilon}_p}{\hat{\varepsilon}_f(\eta, \bar{\theta})} = C = 1, \quad (1)$$

where D is the damage index, $\hat{\varepsilon}_f(\eta, \bar{\theta})$ is the weight coefficient, $d\bar{\varepsilon}_p$ is the equivalent plastic strain increment, $(\eta, \bar{\theta})$ is the current incremental step stress state, C is the damage index at the moment of rupture, and $\overline{\varepsilon_f}$ is the equivalent plastic strain at the moment of rupture.

The result of the weighted integral accumulation of equivalent plastic strain is called damage index D, and $\hat{\varepsilon}_f(\eta, \bar{\theta})$ is the weight factor, also known as "the breaking envelope". It defines the fracture of the material in all states of proportional stress. Equation (2) shows that the material accumulates damage according to the current stress state along the equivalent plastic strain increment at each incremental step. In the fracture criterion, "damage" refers to the loss of ductility of the material, which is not explicitly related to any microscopic volume change. $D = C = 1$ means that "damage" accumulates to the corresponding limit state and ductile fracture begins. $\hat{\varepsilon}_f(\eta, \bar{\theta})$ could be expressed as follows.

$$\hat{\varepsilon}_f = \left\{ \frac{K}{c_2} \left[c_3 + \frac{\sqrt{3}}{2-\sqrt{3}}(1-c_3)\left(\sec\left(\frac{\bar{\theta}\pi}{6} \right) - 1 \right) \right] \times \left[\sqrt{\frac{1+c_1^2}{3}\cos\left(\frac{\bar{\theta}\pi}{6} \right)} + c_1 \left(\eta + \frac{1}{3}\sin\left(\frac{\bar{\theta}\theta\pi}{6} \right) \right) \right] \right\}^{-\frac{1}{n}}, \quad (2)$$

where K is the hardening coefficient, n is the hardening index, c_i is the parameters to be determined, η is the stress triaxiality, and $\bar{\theta}$ is the Rod angle.

Wierzbicki [17] established a relationship between the stress triaxiality and the Rod angle that can reflect the stress triaxiality and Rod angle of a plate in a plane stress state:

$$-\frac{27}{2}\eta\left(\eta^2 - \frac{1}{3}\right) = \sin\left(\frac{\pi}{2}\bar{\theta}\right), \quad (3)$$

where η is the stress triaxiality, and $\bar{\theta}$ is the Rod angle.

3. Experiments

3.1. Material

In this paper, the advanced high-strength dual-phase steel plate DP780 produced by Shanghai Baosteel was utilized as the test material. The plate's thickness was 1 mm, and its chemical composition is presented in Table 1.

Table 1. The chemical composition of DP780 and its mass fraction, %.

Steel	C	Si	Mn	P	S	Alt
DP780	0.1	0.16	2.00	0.014	0.001	0.030

3.2. Uniaxial Tensile Test

In order to study the thermomechanical properties of DP780 steel, the WDW-20D material performance testing machine (Figure 1) was employed to conduct uniaxial tensile tests on DP780 at different temperatures. During the unidirectional tensile tests at different temperatures, the tensile specimen was situated within a heating furnace throughout the process. The heating furnace is comprised of a furnace body, a control system (Figure 2) and a temperature sensor placed in the furnace. This sensor is responsible for recognizing the heating temperature and for setting and reading the temperature, which is controlled by the high-temperature control system. The extensometer is employed to quantify the deformation of the sheet undergoing stretching.

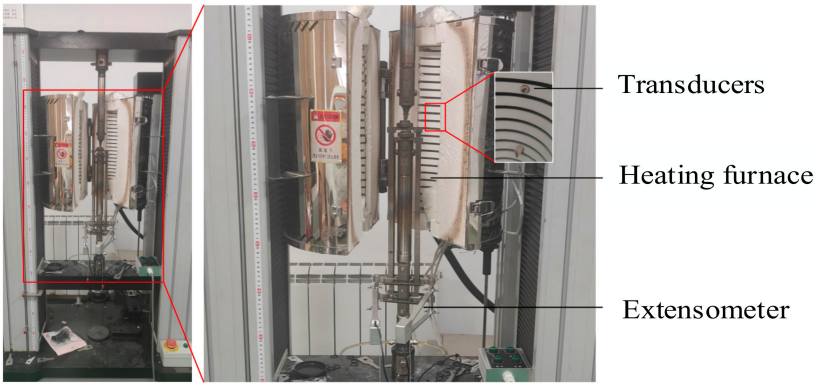


Figure 1. Universal tensile testing machine WDW-20D.



Figure 2. High-temperature furnace control system.

The dimensions of the test specimen were designed in accordance with the China GB/T4338-2006 [17] standard, as illustrated in Figure 3. The specimens were manufactured from the same plate in the direction of plate rolling using laser cutting.

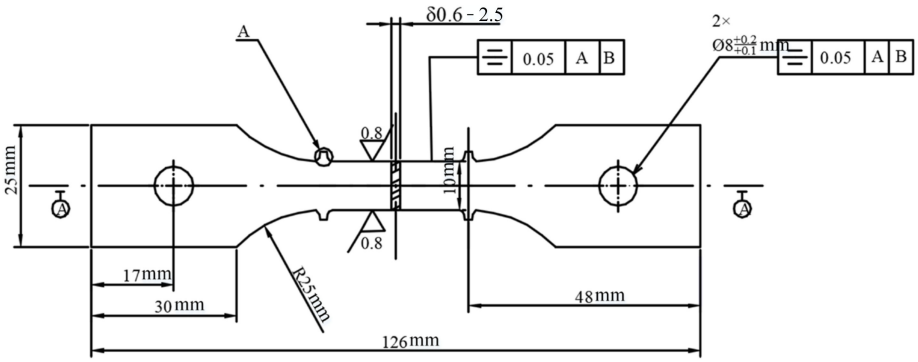


Figure 3. Dimensions of the specimen.

The specimens of dual-phase steel plate were subjected to high-temperature uniaxial tensile tests at 298 K, 473 K, 573 K, 673 K, 773 K, and 873 K, respectively, with a strain rate of 1×10^{-4} s^{-1}. The test results are shown in Figure 4. From the tests, the relevant material property parameters of the steel plate at different tensile temperatures, such as yield strength, tensile strength, and so on, could be directly obtained. The tensile testing machine could directly output the engineering stress–strain curve of the material, which accurately reflected the mechanical characteristics of the material in the plastic deformation stage. The true stress–strain curve of DP780 obtained after its transformation is shown in Figure 5.

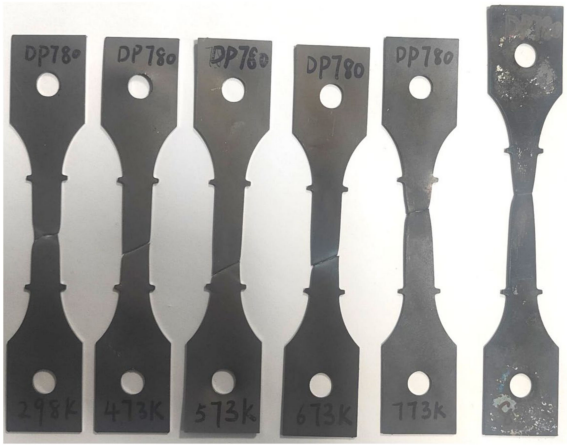


Figure 4. Unidirectional tensile test results of DP780 steel at different temperatures.

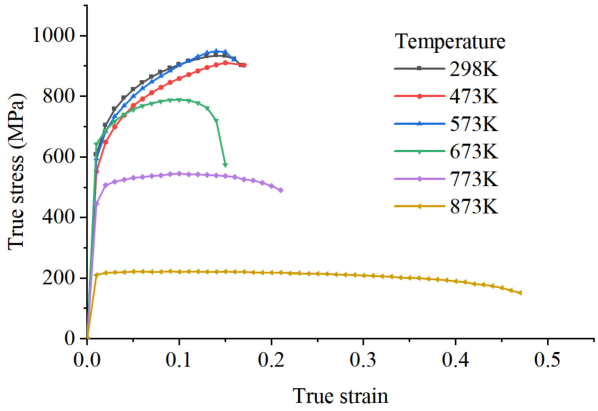


Figure 5. True stress–strain curves in different temperatures.

In this paper, the Swift model was used to fit the stress–strain curve for the uniform extension of its plastic segment, the expression of which is shown in Equation (4). The fitted curves are shown in Figure 6. The values of K and n at different temperatures are shown in Table 2.

$$\sigma = K(\varepsilon_0 + \varepsilon_p)^n, \quad (4)$$

where K is the hardening coefficient, n is the hardening index, ε_0 is the pre-strain, ε_p is the plastic strain, and σ is the stress.

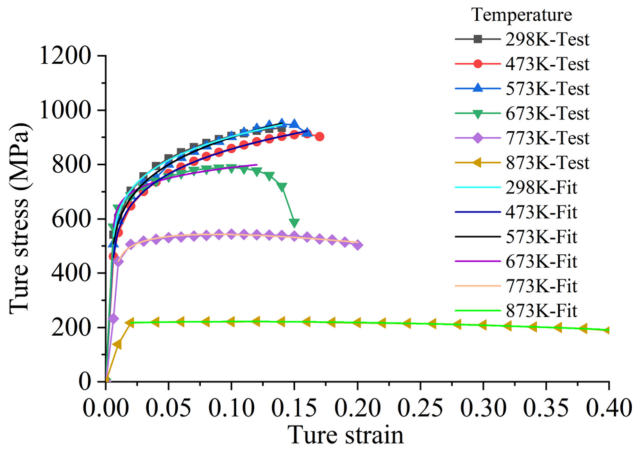


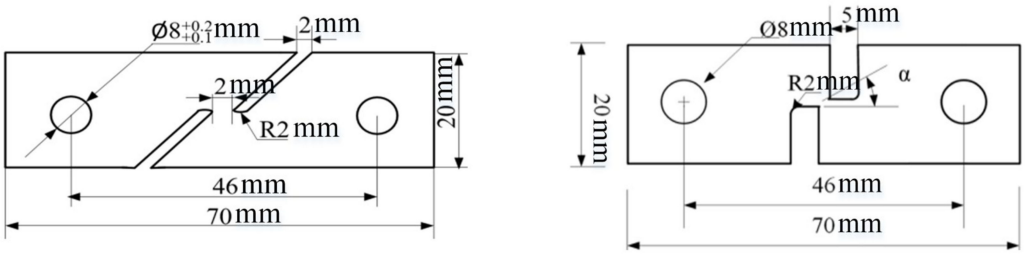
Figure 6. The fitted curves of the Swift model.

Table 2. The K and n of sheet metal at different temperatures.

	298 K	473 K	573 K	673 K	773 K	873 K
K	1305	1700	1518	1015	456.6	257.6
n	0.14	0.21	0.16	0.116	0.076	0.069

3.3. Shear Test

In this paper, 0°, 30°, and 60° shear specimens (shown in Figures 7 and 8) were designed to calibrate the parameters. In order to calculate the pending parameters c_1, c_2, and c_3 of Equation (2), it was necessary to design at least three sets of shear specimens with different stress states to determine the relevant parameters in the criteria. The different angle shear specimens were fixed in the fixture of the tensile testing machine to carry out the corresponding tests, the strain rate was set to 0.0001 s^{-1}, and the shear specimens with different angles were sheared at different temperatures by setting the temperature of the heating furnace on the tensile testing machine.



(**a**) (**b**)

Figure 7. Dimensions of 0° shear specimen (**a**) and other angles (α = 30°, 60°) shear specimens (**b**).

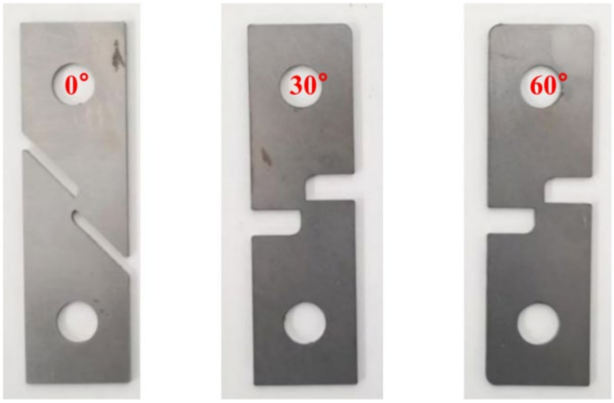
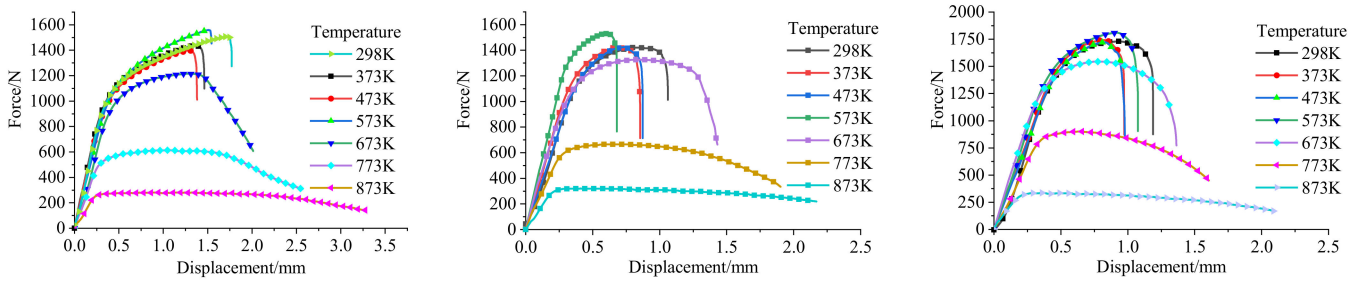


Figure 8. Shear specimens.

The tensile load-displacement curves of shear specimens derived from the tests are shown in Figure 9. From the figure, it can be seen that in the range of 373 K~473 K, the load-displacement curve of the specimen fracture point location difference is very small, indicating that in this temperature range, specimen material-related properties are minimally affected by the temperature. Consequently, in the investigation of the correlation between the pertinent variables and temperature, the data obtained from the room temperature and the temperature range of 473 K to 873 K were employed for the research and analysis.



(**a**) 0° (**b**) 30° (**c**) 60°

Figure 9. Load-displacement curves of shear tests.

4. MMC Model Parameters Calibration

4.1. Parameters Calibration

The MMC criterion in Equation (2) has a hardening coefficient K and hardening index n, as well as c_1, c_2, and c_3 parameters, which need to be obtained through the corresponding tests, where K and n are obtained through the uniaxial tensile test, and to solve the c_1,

c_2 and c_3 parameters, it is necessary to obtain the parameters of stress triaxiality η, Rod angle $\bar{\theta}$, and the equivalent plastic strain ε_p. Since the corresponding parameters cannot be obtained directly through the test, it is necessary to use simulation to obtain them.

In ABAQUS 6.14-4 simulation software, simulation models of shear samples at different angles were established according to the sample specifications mentioned above. The finite element model of the shear specimen at each angle is shown in Figure 10. The four-node shell unit was selected as the model unit in order to obtain more accurate simulation data; the grid in the center region of the specimen was refined, the grid cell size was set to 0.4 mm × 0.4 mm, while the size of the remaining part of the grid cell was set to 1 mm × 1 mm, and the total number of grids was approximately 2800.

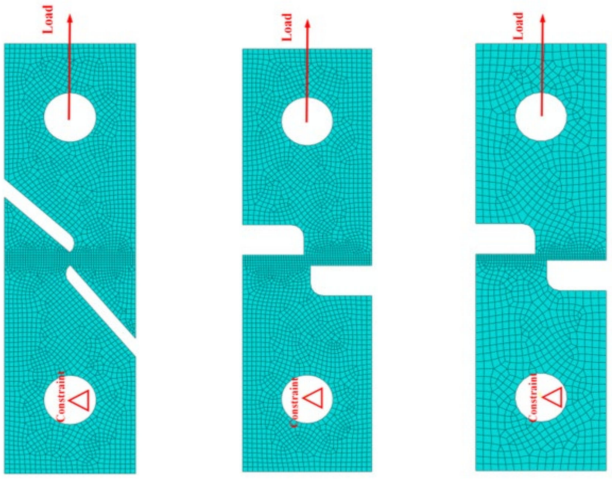
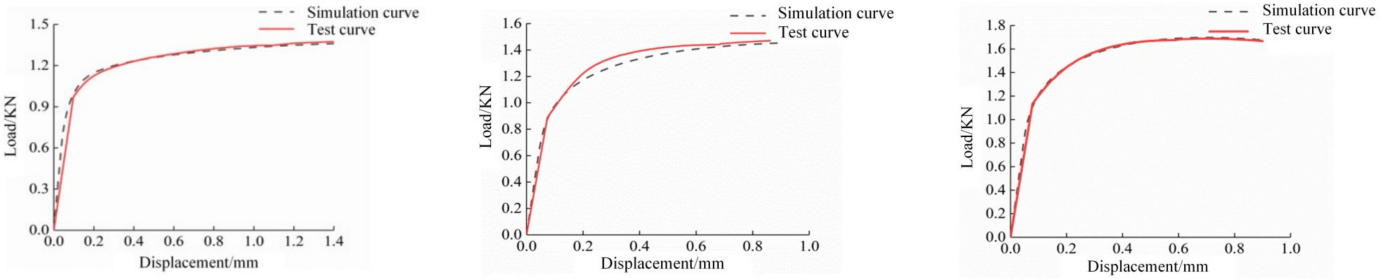


Figure 10. Finite element model of specimens at 0°, 30°, and 60°.

Once the model was established, a tensile test simulation was conducted on the model, resulting in the generation of load-displacement curves. These curves were then compared to the test curves, as illustrated in Figure 11.



(**a**) 0° (**b**) 30° (**c**) 60°

Figure 11. Comparison of specimen simulation and test curves.

The results of the simulation indicate that the equivalent plastic strain and stress triaxiality at the moment of the fracture of the specimen were obtained, as shown in Figure 9, in which the state variable SDV12 represents the equivalent plastic strain in the subroutine, and the center area unit of the specimen at each shear angle is No. 175, No. 98, and No. 166, in this order. Taking the parameter-solving process of DP780 steel at a 673 K temperature as an example, the simulation results of stress triaxiality and equivalent plastic strain at the moment of fracture are shown in the cloud diagram in Figure 12.

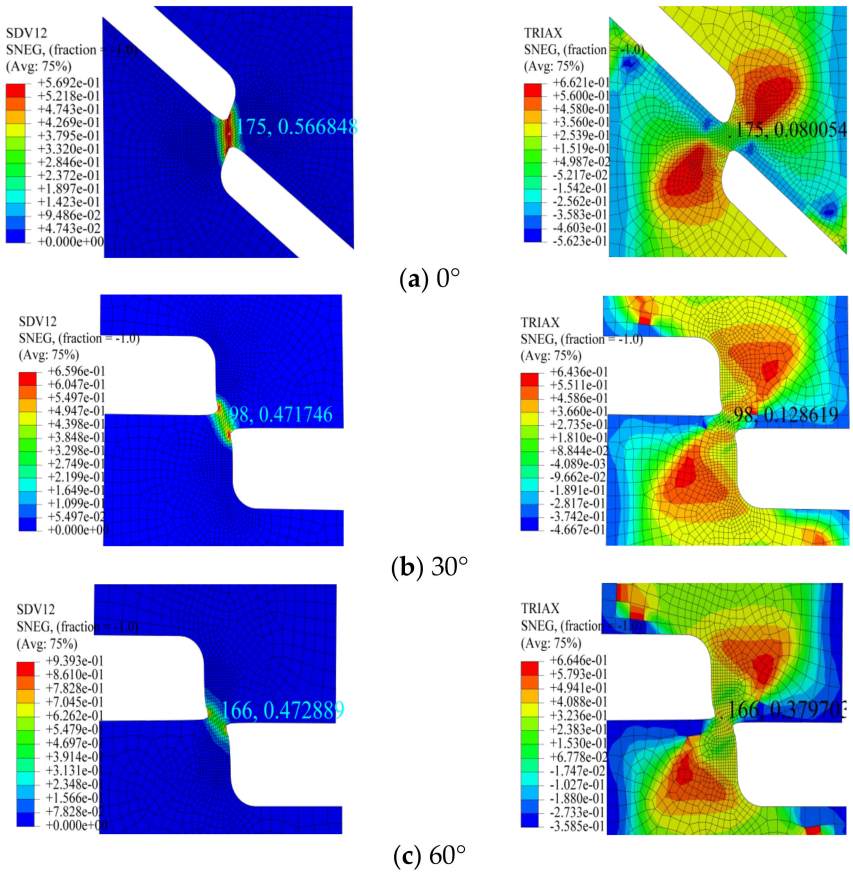


Figure 12. Simulation of stress triaxiality and equivalent strain of sample.

After the simulation was completed, the data of stress triaxiality and equivalent plastic strain of specimens with different angles were derived. From the relationship Equation (3) between stress triaxiality and Rod angle, the corresponding values of Rod angle could be derived. The fracture criterion parameters of the sheet at different temperatures were obtained.

4.2. Simulation Verification

Before applying the failure criterion to the simulation of warm stamping, the failure simulation of the shear test was performed using the derived parameters to verify the accuracy of the calibrated parameters. The MMC criterion was written into the VUMAT subroutine, and the subroutine was called during the finite element simulation. The simulation results are shown in Figure 13, from which it can be seen that the simulated specimen fracture is in the same position as the tested specimen fracture, thereby confirming the accuracy of the solved parameters.

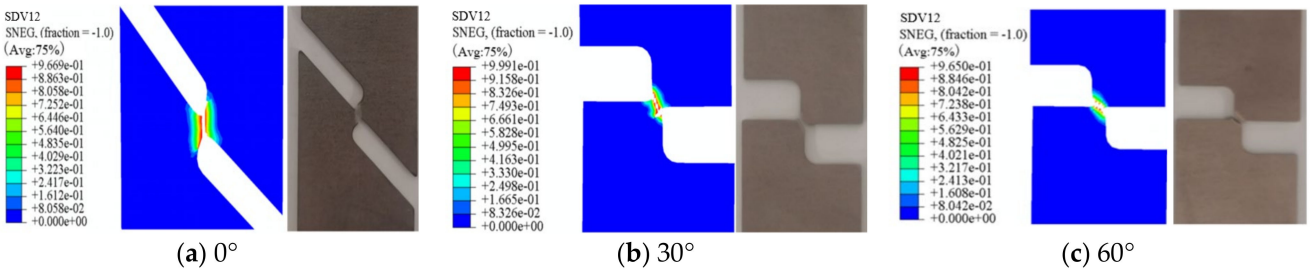


Figure 13. Fracture simulation of shear samples.

4.3. MMC Criterion Parameters versus Temperature

From the temperature dependency of parameters c_1, c_2, and c_3 (Figures 14–16), it can be seen that the c_1 increases with the increase in temperature, and the c_2 decreases with the increase in temperature, and the decrease is larger. The reason is that the c_2 is related to the change in material stress, and with the increase in temperature, the rheological stress of the sheet gradually decreases. The c_3 is linearly dependent on temperature, exhibiting a gradual increase with rising temperatures.

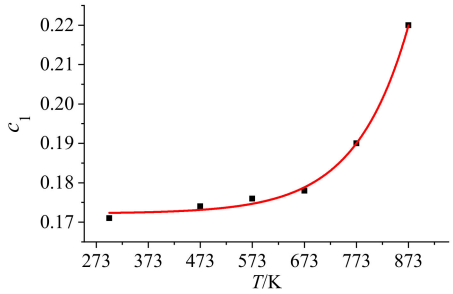


Figure 14. The fitting curve of c_1.

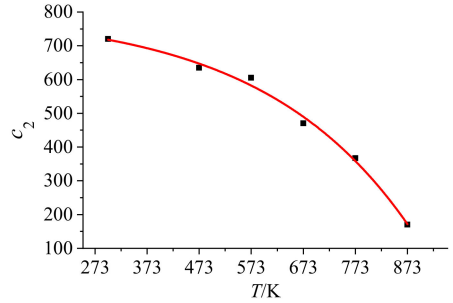


Figure 15. The fitting curve of c_2.

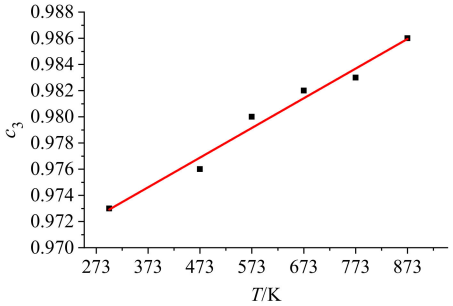


Figure 16. The fitting curve of c_3.

Fitting c_1, c_2, and c_3 to the steel plate temperature using the least squares method yields the following:

$$c_1 = a_1 + b_1 e^{\frac{T}{m_1}}, \tag{5}$$

$$c_2 = a_2 + b_2 e^{\frac{T}{m_2}}, \tag{6}$$

$$c_3 = a_3 T + b_3, \tag{7}$$

where c_1, c_2, and c_3 are the parameters to be determined by the MMC criterion, T is temperature, and a_i, b_i, and m_i are the values of the fitted coefficient. The c_1, c_2, and c_3 fitted equation coefficient values are shown in Table 3.

Table 3. The fitting coefficient value of c_1, c_2, and c_3.

a_1	b_1	m_1	a_2	b_2	m_2	a_3	b_3
0.1722	8.76736×10^{-6}	101.47857	801.40495	−29.21815	284.30263	2.26763×10^{-5}	0.96616

By substituting the fitted MMC criterion parameters into Equation (2), an expression for the MMC criterion considering the effect of temperature can be obtained:

$$\hat{\varepsilon}_f = \left\{ \frac{K}{a_2 + b_2 e^{\frac{T}{m_2}}} \left[(a_3 T + b_3) + \frac{\sqrt{3}}{2-\sqrt{3}} (1 - (a_3 T + b_3)) \left(\sec\left(\frac{\overline{\theta}\pi}{6} \right) \right) \right] \right. \\ \left. \times \left[\sqrt{\frac{1 + \left(a_1 + b_1 e^{\frac{T}{m_1}} \right)}{3}} \cos\left(\frac{\overline{\theta}\pi}{6} \right) + \left(a_1 + b_1 e^{\frac{T}{m_1}} \right) \left(\eta + \frac{1}{3} \sin\left(\frac{\overline{\theta}\pi}{6} \right) \right) \right] \right\}^{-\frac{1}{n}}, \quad (8)$$

where η is the stress triaxiality, $\overline{\theta}$ is the Rod angle, $\hat{\varepsilon}_f$ is the equivalent plastic strain, K is the hardening coefficient, n is the hardening index, T is temperature, and a_i, b_i, and m_i is the value of the fitted coefficient.

5. Stretch-Bending Tests and Simulation

5.1. Stretch-Bending Tests

In order to ascertain the accuracy of Equation (8) in predicting the fracture of dual-phase steel plates at the fillet of the punch at different temperatures, a series of stretch-bending tests on U-shaped components was designed. The test was conducted using a variety of fillet radius stamping models to simulate the potential shear fracture and tension-shear composite fracture of steel plates.

The CNC hydraulic press selected for the test was the YZ32-160S, which is comprised primarily of a die, punch, holder, draw bead, and other components, as illustrated in Figure 17. Specimens with fillet radii of 1 mm, 5 mm, and 10 mm were designed for the purpose of conducting forming tests.

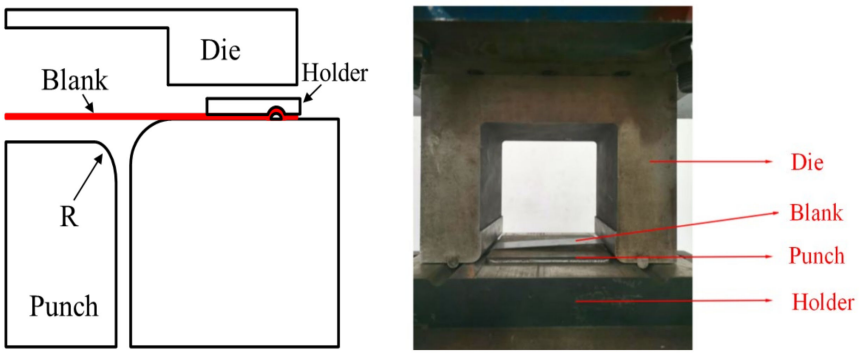


Figure 17. Specimen stretch-bending die.

Prior to the stamping test, the plate specimen was subjected to a heating process at a temperature of 723 K using a high-temperature furnace and maintained at this temperature for a period of five minutes. The sheet was positioned on the stamping die, and the specimen was initially crimped using a die, followed by the application of pressure from the hydraulic press to eject the punch. Upon the rupture of the specimen at the edge, the stamping process was terminated, and the ejection height was duly recorded. The fracture of the specimen at different fillet angles of the punch is illustrated in Figure 18.

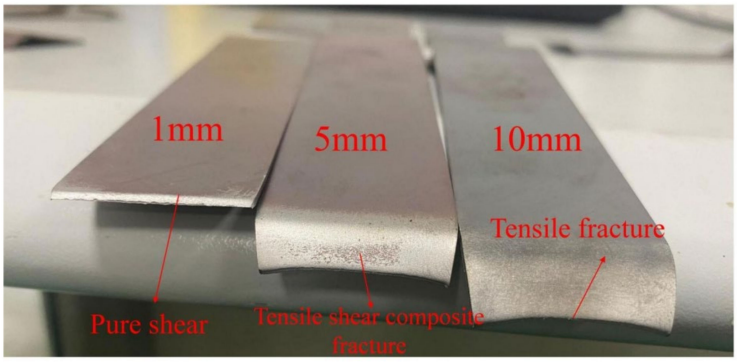


Figure 18. Specimen fracture position.

As illustrated in Figure 15, the specimen primarily experiences rupture failure during the stretch-bending tests in the vicinity of the fillet of the punch. When the radius of the punch fillet is 1 mm, the fracture of the specimen is relatively straight, and there is no obvious necking phenomenon, as shown in Figure 19a, which demonstrates that the fracture of the dual-phase steel at the small fillet in the stamping process is a shear fracture. When the radius of the punch fillet is increased to 5 mm, necking starts to appear at the fracture, as shown in Figure 19b, which is a mixed fracture in tension and shear. Upon increasing the radius of the punch fillet to 10 mm, it becomes evident that there is a distinct necking and thinning at the fracture, as shown in Figure 19c, which indicates that the fracture of the specimen here is a tensile fracture. Additionally, it demonstrates that the stress state at the fracture of the specimen undergoes a transition from pure shear to a combination of tension-shear as the radius of the punch fillet increases.

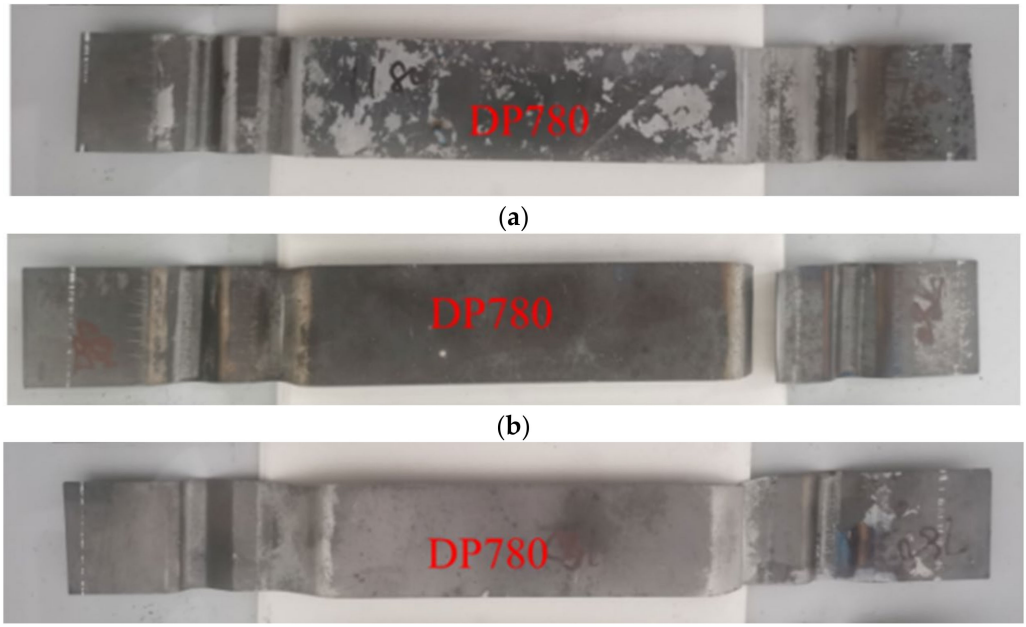


Figure 19. Fracture diagram of stretch-bending specimen. (**a**) Fracture specimens with a 1 mm radius of fillet. (**b**) Fracture specimens with a 5 mm radius of fillet. (**c**) Fracture specimens with a 10 mm radius of fillet.

5.2. Stretch-Bending Simulation Verification

The simulation model of the stretch-bending tests of the U-shape component was constructed in ABAQUS, as shown in Figure 20. The punch and die were defined as rigid bodies due to their inherent difficulty in undergoing deformation. This designation served

to enhance the computational efficiency of the model. The sheet unit was designated as the shell unit of S4R, the size of the divided grid cell was 1 mm × 1 mm, and the overall number of cells was 23,907. The size of the punch fillet was changed to achieve the tension fracture of the plate in different fillet radii with a plate thickness of 1 mm. A simulation called the VUMAT subroutine contained the MMC fracture criterion.

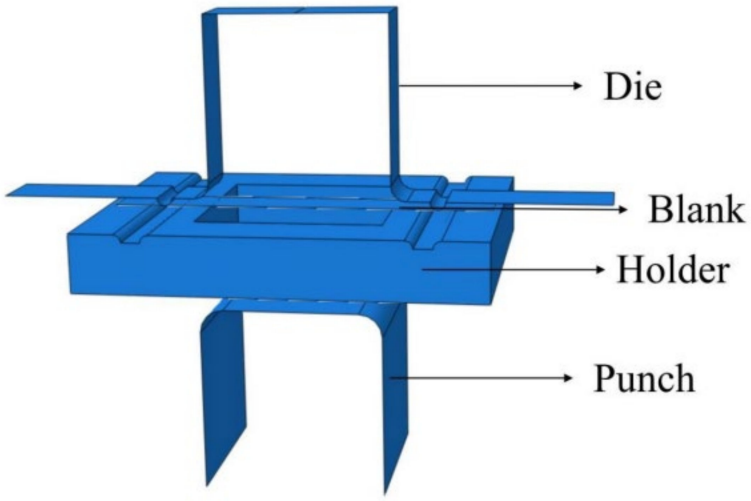


Figure 20. Stretch-bending mold model.

Once the model has been established, a bending test simulation was conducted on the model, and the load-displacement curve of the punch after simulation was obtained and compared to the test curve, as illustrated in Figure 21. The discrepancy between the test and simulation results was minimal.

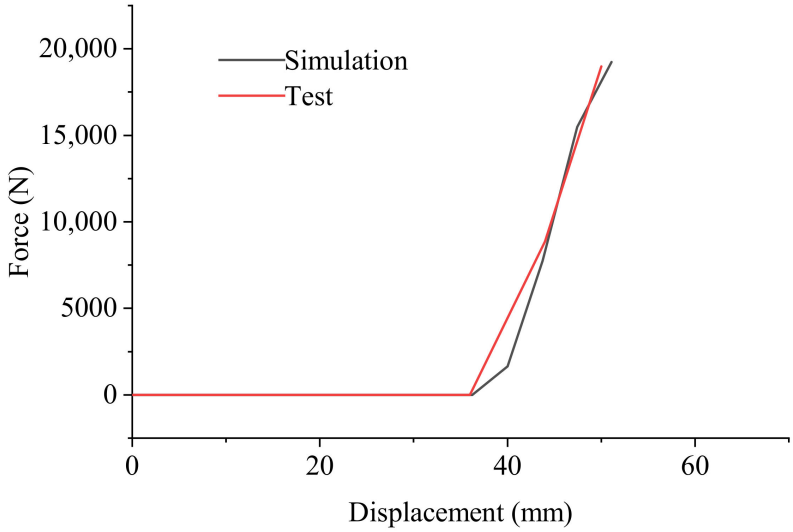
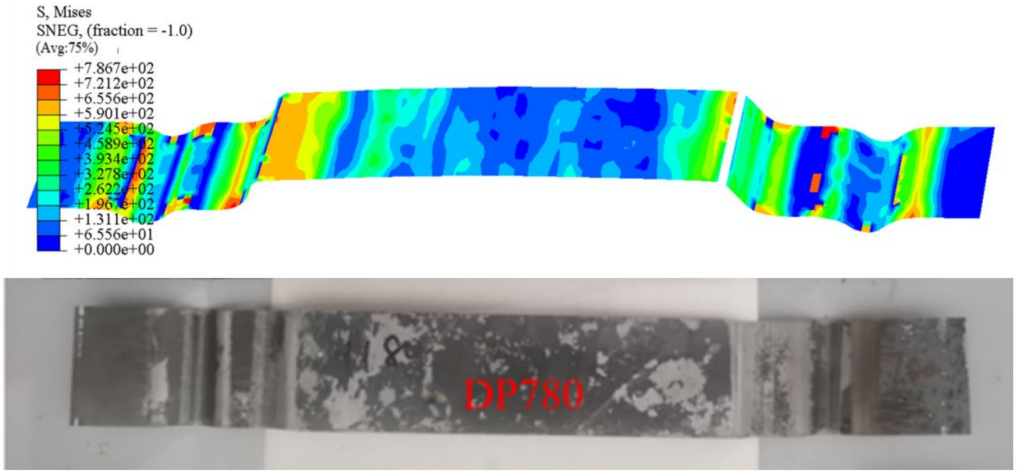
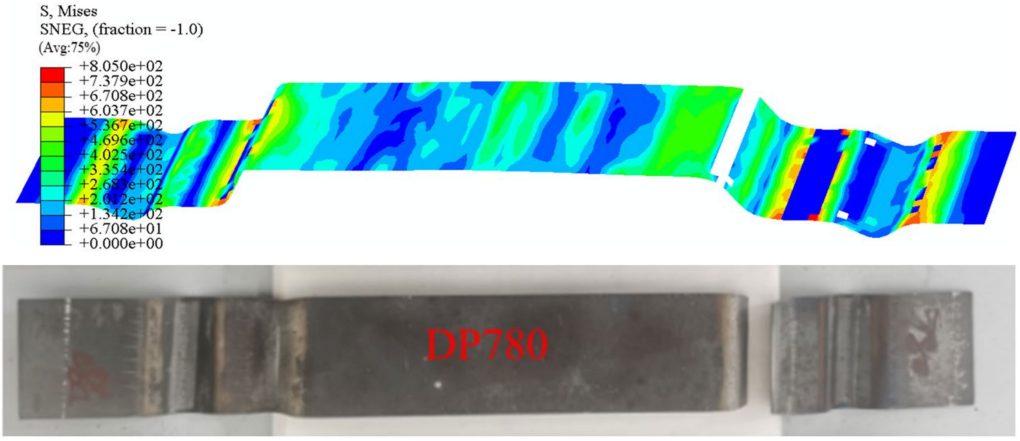


Figure 21. Comparison of punch simulation and test curves.

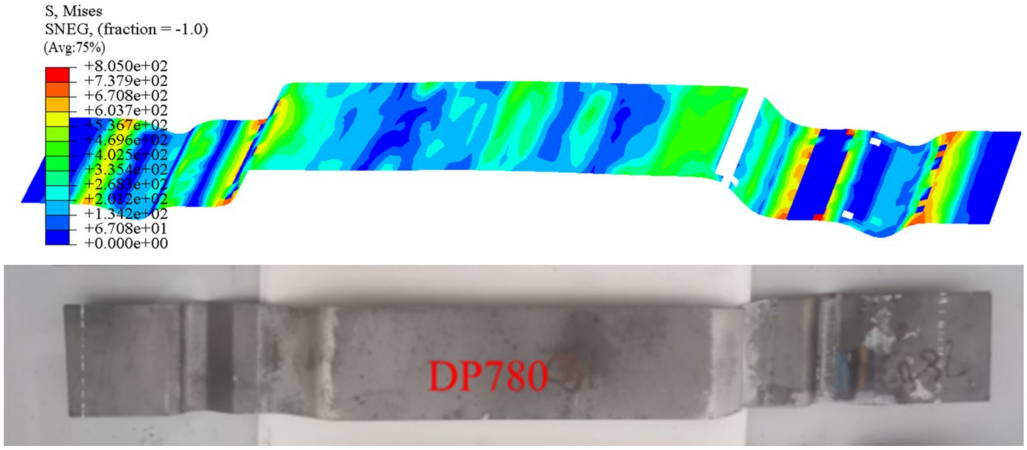
The simulation results of steel plate stamping when the radius of the punch fillet was 1 mm, 5 mm, and 10 mm are shown in Figure 22, from which it can be seen that the simulated fracture location and fracture morphology are similar to the test results. Table 4 provides a comparison between the simulation and test results. A comparison of the simulation and test results indicates that the discrepancy between the simulated and tested forming depths is minimal, suggesting that Equation (8) can accurately predict the fracture at the fillet under the conditions of warm stamping.



(**a**) R = 1 mm



(**b**) R = 5 mm



(**c**) R = 10 mm

Figure 22. Comparison of stretch-bending test and simulation.

This paper successfully calibrated the MMC criterion parameters of the DP780 sheet at different temperatures and established a relationship between the parameters and temperature, ranging from 298 K to 873 K. This addresses the issue in previous literature that the MMC criterion can only predict rupture under room temperature conditions and demonstrates the applicability of the MMC criterion for predicting rupture under warm forming.

Table 4. The depth of punch with different fillet radius.

Punch Fillet Radius R_p (mm)	Test Press Depth d_1 (mm)	Simulation of Stamping Depth d_2 (mm)	Error
1	8.7	9.2	5.7%
5	10.8	9.9	8.3%
10	12.4	11.7	5.6%

6. Conclusions

It is of significant importance to conduct the calibration of MMC parameters at varying temperatures and to study the relationships between parameters and temperature in order to predict rupture failure. Firstly, the temperature-dependent stress–strain relationship of dual-phase steel was determined through the uniaxial tensile test conducted at temperatures ranging from 298 K to 873 K. This relationship was fitted based on the Swift model to obtain the mechanical property parameters at different temperatures. Secondly, a series of shear tests were conducted on dual-phase steel at various angles within the temperature range of 298 K to 873 K. The tests were performed at different temperatures, and the relevant parameters (such as stress triaxiality, Rod angle, and equivalent fracture strain) of the steel plate in different stress states were obtained by combining finite element simulation with the results of the tests. The obtained parameters were incorporated into the MMC criterion, where the undetermined parameters were identified through the resolution of the associated system of equations. The relationship between each parameter in the criterion and the temperature was investigated, and the validity of the relationship between criterion parameters and temperature was verified using stretch-bending tests of the U-shape part.

In the context of the automotive parts stamping process, temperature forming can be employed to effectively enhance material elongation and improve its molding performance. When stamping at a specific temperature, in accordance with the criterion parameters obtained in this paper and the temperature correlation curves, we can derive the corresponding temperature fracture parameters. The VUMAT subroutine, which contains the MMC fracture criterion, is called during the Abaqus simulation. This enables the parts of the actual stamping process to be guided significantly more effectively, thereby reducing the development cycle and production cost.

The main conclusions of this study are the following:

1. The parameters of the MMC criterion at different temperatures were calibrated by combining the numerical results of the DP780 shear test with experimental data;
2. By fitting the correlation curves of the MMC criterion parameters c_1, c_2, and c_3 with the temperature, the law of the criterion parameters changing with temperature in the temperature range of 298 K~873 K was determined, and the expression of the MMC criterion considering the effect of temperature was established.

Author Contributions: Conceptualization, Y.L. and D.L.; methodology, Y.L. and H.S.; software, H.S. and D.W.; validation, D.W. and Y.W.; formal analysis, Y.L., Y.W. and H.S.; investigation, Y.L., D.W. and Y.W.; resources, D.L.; data curation, D.L. and H.S.; writing—original draft preparation, Y.L. and H.S.; writing—review and editing, Y.L. and D.L.; visualization, H.S. and Y.W. and D.W.; supervision, D.L.; project administration, D.L. All authors have read and agreed to the published version of the manuscript.

Funding: The Project supported by China National Natural Fund (12302182) and China Sino Truck Group industry-university-research cooperation program project (No. 20200810).

Data Availability Statement: The raw data supporting the conclusions of this article will be made available by the authors on request.

Conflicts of Interest: The authors declare no conflict of interest.

References

1. Lian, J.; Sharaf, M.; Archie, F.; Münstermann, S. A hybrid approach for modelling of plasticity and failure behaviour of advanced high-strength steel sheets. *Int. J. Damage Mech.* **2013**, *22*, 188–218. [CrossRef]
2. Jin, X.; Gong, Y.; Han, X. Research status and Prospect of Advanced Thermoforming Automotive Steel Manufacturing and Application. *Acta Met. Sin.* **2019**, *56*, 411–428. (In Chinese)
3. Wang, S.; Yu, H.; Chen, M. Comparative analysis of B-column hot-forming Technology for Automobile. *J. Plast. Eng.* **2019**, *26*, 70–76. (In Chinese)
4. Fu, Q. *Research on Failure Stress Type Criterion of Advanced High Strength Duplex Steel Sheet Forming*; Shandong University of Science and Technology: Zibo, China, 2023. (In Chinese)
5. Li, S.; He, J.; Gu, B.; Zeng, D.; Xia, Z.C.; Zhao, Y.; Lin, Z. Anisotropic fracture of advanced high strength steel sheets: Experiment and theory. *Int. J. Plast.* **2018**, *103*, 95–118. [CrossRef]
6. Li, Y.; Luo, M.; Gerlach, J.; Wierzbicki, T. Prediction of shear-induced fracture in sheet metal forming. *J. Mater. Process. Technol.* **2010**, *210*, 1858–1869. [CrossRef]
7. Bai, Y.; Wierzbicki, T. A new model of metal plasticity and fracture with pressure and Lode dependence. *Int. J. Plast.* **2008**, *24*, 1071–1096. [CrossRef]
8. Bai, Y.; Wierzbicki, T. Application of extended Mohr-Coulomb criterion to ductile fracture. *Int. J. Fract.* **2010**, *161*, 1–20. [CrossRef]
9. Bai, Y.; Wierzbicki, T. A comparative study of three groups of ductile fracture loci in the 3D space. *Eng. Fract. Mech.* **2015**, *135*, 147–167. [CrossRef]
10. Ji, C.; Li, Z.; Liu, J. Development of an improved MMC-based fracture criterion characterizing the anisotropic and strain rate-dependent behavior of 6061-T5 aluminum alloy. *Mech. Mater.* **2020**, *150*, 103598. [CrossRef]
11. Granum, H.; Morin, D.; Børvik, T.; Hopperstad, O.S. Calibration of the modified Mohr-Coulomb fracture model by use of localization analyses for three tempers of an AA6016 aluminium alloy. *Int. J. Mech. Sci.* **2021**, *192*, 106122. [CrossRef]
12. Luo, M.; Wierzbicki, T. Numerical failure analysis of a stretch-bending test on dual-phase steel sheets using a phenomenological fracture model. *Int. J. Solids Struct.* **2010**, *47*, 3084–3102. [CrossRef]
13. Pack, K.; Luo, M.; Wierzbicki, T. Sandia Fracture Challenge: Blind prediction and full calibration to enhance fracture predictability. *Int. J. Fract.* **2014**, *186*, 155–175. [CrossRef]
14. Dunand, M.; Mohr, D. On the predictive capabilities of the shear modified Gurson and the modified Mohr–Coulomb fracture models over a wide range of stress triaxialities and Lode angles. *J. Mech. Phys. Solids* **2011**, *59*, 1374–1394. [CrossRef]
15. Huang, G.; Zhu, H.; Sriram, S.; Chen, Y.; Xia, Z.C.; Faruque, O. Fracture Prediction and Correlation of AlSi Hot Stamped Steels with Different Models in LS DYNA. In Proceedings of the 13th International LS-DYNA Users Conference, Detroit, MI, USA, 8 June 2014.
16. Lou, Y.; Huh, H. Prediction of ductile fracture for advanced high strength steel with a new criterion: Experiments and simulation. *J. Mater. Process. Technol.* **2013**, *213*, 1284–1302. [CrossRef]
17. *GB/T4338-2006*; Metallic Materials High Temperature Tensile Test Method. General Administration of Quality Supervision, Inspection and Quarantine of the People's Republic of China, Standardization Administration of China: Beijing, China, 2006. (In Chinese)

Disclaimer/Publisher's Note: The statements, opinions and data contained in all publications are solely those of the individual author(s) and contributor(s) and not of MDPI and/or the editor(s). MDPI and/or the editor(s) disclaim responsibility for any injury to people or property resulting from any ideas, methods, instructions or products referred to in the content.